Structure and Properties of Gelatin Methacryloyl (GelMA) Synthesized in Different Reaction Systems

Shangsi Chen [a 1], Yue Wang [a 1], Jiahui Lai [a], Shenglong Tan [b, c, *], Min Wang [a, *]

[a] Department of Mechanical Engineering
The University of Hong Kong
Pokfulam Road, Hong Kong

[b] Department of Endodontics, Stomatological Hospital
Southern Medical University
Guangzhou, China

[c] School of Stomatology
Southern Medical University
Guangzhou, China

Keywords: GelMA synthesis, physical structure, photocurable efficiency, tissue engineering, 3D bioprinting

* Corresponding Authors:
Professor Min Wang, at the University of Hong Kong, Hong Kong, China
Email: memwang@hku.hk Tel: +852 3971 7903 Fax: +852 2858541
Dr. Shenglong Tan, at the Stomatological Hospital of Southern Medical University, Guangzhou, China
Email: tansl@hust.edu.cn
[1] These authors contributed equally to this work

Abstract

Gelatin methacryloyl (GelMA) hydrogels have been extensively used for drug delivery and tissue engineering applications due to their good biocompatibility, biodegradability, and controllable photocurable efficiency. Phosphate buffer solution (PBS) is the most widely used reaction system for GelMA synthesis. However, carbonate-bicarbonate buffer solution (CBS) has been tried recently for synthesizing GelMA due to its high reaction efficiency. But there is a lack of systematic investigation into possible differences in the structure and properties of GelMA synthesized in PBS and CBS, respectively. Therefore, in the current study, GelMA molecules with two degrees of methacryloylation (~20% and ~80%) were synthesized under PBS and CBS reaction systems, respectively, in comparable conditions. The results showed that because of the functionalization of methacrylate groups in gelatin chains, which can interfere with the intrachain and interchain interactions, such as hydrogen bonding, the GelMA molecules synthesized in PBS had distinct physical structures and exhibited different properties in comparison with those produced in CBS. GelMA hydrogels synthesized in PBS exhibited a higher gel-sol transition temperature and better photocurable efficiency, mechanical strength, and biological properties. In contrast, GelMA hydrogels produced in CBS showed advantages in swelling performance and microstructures, such as pore size and porosity. In addition, GelMA synthesized in PBS and possessing a high degree of methacryloylation (the “GelMA-PH” polymer) showed great potential for 3D bioprinting. This focused study has gained helpful new insights into GelMA and can provide guidance on the application of GelMA in 3D printing and tissue engineering.

1. Introduction

Given their highly dynamic polymer networks, which can respond easily to the internal and external stimuli, the application of hydrogels in controlled drug release has gained tremendous attention over the past few decades [1-3]. Additionally, hydrogels have been extensively used in wound dressing and tissue engineering because of their hydrophilic polymer network with high water content, similar to the extracellular matrix (ECM) of human body tissues, excellent biocompatibility, and tunable physicochemical properties [4-7]. Typically, hydrogels can be categorized into those composed of synthetic polymers and those composed of natural polymers. Hydrogels formed by synthetic polymers usually possess higher mechanical strength and stiffness and lower degradation rates than those by natural polymers [8]. In contrast, hydrogels from natural polymers exhibit excellent biocompatibility and biodegradability and the potential to simulate the structure and function of ECM for modulating cell behaviors. Consequently, natural polymer-based hydrogels have gained more interest in biomedical applications [6, 9-12].

Among a variety of natural polymer-based hydrogels, gelatin-based hydrogels play an important role in biomedical applications due to their remarkable biocompatibility [13-16]. Gelatin (Gel) is a denatured protein obtained by the hydrolysis of collagen. It has the Arg-Gly-Asp (RGD) sequence that can interact with cell integrins to improve cell behaviors, including cell adhesion, migration, proliferation, and differentiation and exhibits no immunogenicity [17-20]. Although gelatin hydrogels have attracted significant interest in tissue engineering, some intrinsic limitations, such as inadequate mechanical

strength and rapid degradation, have hindered their biomedical applications. Fortunately, gelatin has many active side chains, such as -OH, -NH2, -COOH, which allows the possibility for it to react with specific groups via chemical modifications to overcome the aforementioned disadvantages [15, 21, 22]. For example, gelatin methacryloyl (GelMA) is an engineered gelatin-based biomaterial obtained by the methacrylation of the lysine groups in the gelatin backbone [21, 23, 24]. Apart from excellent biocompatibility, biodegradability, and the presence of RGD sequence, GelMA can be covalently crosslinked with water-soluble photoinitiators upon exposure to visible or ultraviolet (UV) light to form stable hydrogels. Crosslinked GelMA hydrogels can maintain structural stability at the body temperature, offering wide avenues for applications in tissue engineering and drug delivery [25-27]. Furthermore, in contrast to pure gelatin, GelMA possesses tailorable mechanical strength and biodegradation rate owing to its photocurable property.

The synthesis of GelMA was firstly reported by Van Den Bulcke *et al*. in 2000 under the reaction system of phosphate buffer solution (PBS), where GelMA could be synthesized through the reaction of gelatin with methacrylic anhydride (MA) [24]. Many studies have showed that the degree of substitution (DS) or the degree of methacryloylation (DM) in GelMA could be adjusted via the feed ratio of MA to gelatin, resulting in controlling the biophysiochemical properties of the synthesized GelMA [28-31]. Recently, as the demand for GelMA escalates drastically, GelMA has been made commercially available. According to some suppliers, such as Sigma-Aldrich, the mainstream GelMA synthesis method is under the PBS reaction system. However, there

is a strong interest in investigating more effective ways to prepare GelMA with controllable biophysiochemical properties. Several research groups have reported some other methods for GelMA synthesis. For instance, recent investigations have pointed out that GelMA synthesized under the carbonate-bicarbonate buffer solution (CBS) was superior to those synthesized in PBS in the context of rendering the deprotonation of free amino groups and buffering capability [32-34]. Moreover, the MA amount needed for GelMA synthesis was less under the CBS reaction system, making GelMA synthesis environmentally friendly and also cost-effective.

Nowadays, increasing efforts are made to apply GelMA synthesized by different methods to drug delivery, tissue engineering, and 3D bioprinting [26, 35, 36]. At the same time, there is a lack of systematic studies to compare the structure and properties, such as physical structure, temperature-sensitive behavior, and UV-crosslinking efficiency, of GelMAs made by different synthesis methods. Therefore, it is necessary to investigate systematically the structure and properties of GelMAs synthesized by different methods. In the current study, four sets of GelMAs with two DS (high and low) under PBS or CBS reaction system were synthesized via a one-pot synthesis strategy. Subsequently, research was conducted to reveal the differences between obtained GelMA in terms of methacryloylation, physical structure, rheological properties, UV crosslink ability, swelling behavior, mechanical strength, and biological properties. It was shown that the GelMA synthesized under the CBS reaction system required less amount of MA than those under PBS. However, due to the difference in physical structures, GelMA synthesized under the PBS reaction system had a higher gel-sol

89 transition temperature than those under CBS. Moreover, the photocurable properties of
90 GelMA synthesized under the PBS reaction system were more effective than those
91 under CBS. Furthermore, 3D printed cell-laden GelMA hydrogel was successfully
92 constructed, indicating great potential of synthesized GelMA for 3D bioprinting.

2. Materials and methods

2.1 Materials

Gelatin (porcine skin, type A, powder, gel strength ~300 g Bloom), methacrylate anhydride (MA, 94%), 2-hydroxy-2-methylpropiophenone (97%), sodium dodecyl sulphate (SDS), glycine, 2,4,6-Trinitrobenzenesulfonic acid (TNBS), and deuterium oxide were bought from Sigma-Aldrich (St. Louis, MO, USA). Dialysis tubing cellulose membrane (MWCO 10 kDa) was purchased from Thermo Fisher Scientific (USA). Dulbecco's modified eagle medium (DMEM), fetal bovine serum, and penicillin-streptomycin (10,000 U/ml) were supplied by Gibco (Thermo Fisher Scientific, USA). The live/dead assay kits were purchased from Invitrogen (Thermo Fisher Scientific, USA). All reagents were used as-received without further purification.

2.2 Synthesis of GelMA

In the current study, four sets of GelMA with two degrees of substitution (~20% DS as low methacrylation and ~80% DS as high methacrylation) were synthesized under PBS and CBS reaction systems, respectively, based on previously described protocols [32, 33, 37]. According to the different reaction systems and DS, GelMA synthesized was designated as GelMA-PH, GelMA-PL, GelMA-CH, and GelMA-CL, respectively. For instance, GelMA-PH refers to GelMA synthesized in PBS and had a high degree of substitution. It was shown previously that several parameters could significantly affect the DS for GelMA synthesis, including the pH of reaction medium, duration of reaction, and MA amount [32, 37]. Therefore, in the current study, the DS of synthesized GelMA was controlled by regulating these parameters, i.e., pH, duration of reaction and MA

amount. For GelMA-PH or GelMA-PL synthesis, briefly, 10g gelatin was dissolved in 100ml PBS (0.01M, pH 7.4, 0.137 M NaCl, 2.7 mM KCl, 10mM Na_2HPO_4, 1.8 mM KH_2PO_4) at 50℃ water baths. 8.0ml or 0.8ml MA was added into the gelatin solution dropwise at a rate of 0.5ml/min under constant magnetic stirring. After reacting for 1h, 500ml PBS was added to stop the reaction. Afterwards, the solution was transferred into the dialysis tube (10 kDa MWCO) to dialyze against deionized (DI) water for 7 days at 40℃. The DI water was refreshed daily to fully remove the salts and MA totally. GelMA was obtained via lyophilization and stored at 4℃ until further use.

For GelMA-CH or GelMA-CL synthesis, 10g gelatin was dissolved in 100ml 0.25M CBS (pH 9.0, 0.239 M $NaHCO_3$, 0.0114 M Na_2CO_3) at 50℃ water baths. The pH of the gelatin solution was tuned to 9 by 5N NaOH solution. 1.0ml or 0.2ml MA was added into the above solution dropwise. After MA addition, the solution pH was adjusted to 9 again. After reacting for 1h, the final pH of the reaction system was adjusted to 7.4 using 1M HCl. Afterwards, the solution was transferred into the dialysis tube (10 kDa MWCO) to dialyze against deionized (DI) water for 7 days at 40℃. GelMA was obtained via lyophilization and stored at 4℃ until further use.

2.3 Degree of substitution and characterization of GelMA

To quantify the degree of substitution for GelMA, ^{1}H-NMR spectroscopy (Bruker Avance III 400, USA) and TNBS assay were conducted. For ^{1}H-NMR spectroscopy analysis, gelatin, GelMA-PH, GelMA-PL, GelMA-CH, and GelMA-CL were dissolved in deuterium oxide at 20mg/ml concentration at 50℃, and the 1H chemical shifts of each sample were recorded. For the TNBS method, 500μL 1.6mg/ml gelatin and

GelMA were dissolved in 0.1M sodium bicarbonate solution and then added in 2ml EP tubes, respectively. Subsequently, 500μL 0.2% TNBS solution was added, and the tubes were placed in 37℃ for 3h. Then, 250μL 1M HCl and 500μL 10% SDS solution were added in the tubes to stop the reaction. The OD value of gelatin and GelMA samples was measured at 335nm wavelength using a UV–vis spectrophotometer (UV-2600, Shimadzu, Japan). The molar concentration of free primary amino groups in gelatin and GelMA was calculated based on the glycine calibration curve (Fig.S1).

Additionally, the synthesized GelMA was characterized using an X-ray diffractometer (XRD, 7000S, Shimadzu, Japan) over a range of 2θ from 0° to 60° and FT-IR spectrometer (PerkinElmer, USA) under the attenuated total reflection (ATR) mode.

2.4 Phase transition temperature of GelMA

To investigate the effect of reaction environment and methacrylation degree on GelMA structure, the gel-sol transition temperature of GelMA was studied. Taking gelatin as the control, 5.0% w/v GelMA was dissolved in PBS. The sol-gel transition of gelatin and GelMA solutions was monitored from 4℃ to 40℃ using a Rheometer (MCR 302, Anton Paar, Austria) equipped with a parallel plate unit with a 20 mm diameter (1% strain and 1 Hz).

2.5 Circular dichroism (CD) spectroscopy

To determine the secondary structure in GelMAs synthesized in PBS and CBS, respectively, CD experiments (UV wavelength, 260-185 nm) were conducted using a CD spectrometer (JASCO J-815, Japan). 0.2 mg/ml gelatin and GelMA samples were dissolved in DI water and stored at room temperature. After adding 300μL of gelatin or

GelMA solution, quartz cell was placed at 4, 20, or 37℃ for 30min to obtain a stable conformation (triple helix or random coil structure). Then, CD spectra were obtained with 5 accumulations and an optical path length of 1nm. At least three independent measurements were conducted for each solution.

2.6 GelMA hydrogels preparation

GelMA hydrogels were prepared by dissolving 0.5% v/v 2-hydroxy-2-methylpropiophenone photoinitiator in DI water at 50℃ water bath and following the dissolution of GelMA-PH, GelMA-PL, GelMA-CH, and GelMA-CL at the concentration of 5% w/v. Subsequently, GelMA solutions were cooled down to room temperature. Then, GelMA samples were exposed to a UV lamp (360mW) at 365nm wavelength for different time intervals (0s, 60s, 120s, 240s, and 480s) to construct GelMA hydrogels.

2.7 Characterization and evaluation of GelMA hydrogels

2.7.1 Rheological properties

The rheological properties of GelMA hydrogels were investigated at 20℃ using a Rheometer. According to the preliminary strain sweep test results, GelMA hydrogels were loaded onto a parallel plate and subjected to a shear strain (γ) of 1.0% at a 0.5mm gap under continuous oscillation. In the frequency sweep mode, the storage moduli (G') and loss moduli (G") of GelMA hydrogels were measured in the range of 0.1 - 100 rad/s.

2.7.2 Surface morphology and structure

GelMA hydrogels crosslinked via the UV light were freezing-dried and sputter-coated with a layer of gold particles. Afterwards, GelMA samples were examined under a

scanning electron microscope (SEM, Hitachi S4800, Japan) to observe the surface morphology in high vacuum mode at 10kV. Additionally, the GelMA samples' surface pore size and pore area percent were analyzed using the Image J software.

2.7.3 Porosity

The porosities of freezing-dried GelMA samples were measured based on the Archimedes principle [38]. Initially, the weight of lyophilized GelMA samples and the pycnometer bottle full of absolute ethanol were weighed using a digital balance and named M_S and M_1, respectively. Subsequently, the dried GelMA samples were soaked in the pycnometer bottle and vacuumed until GelMA samples were full of ethanol. The pycnometer bottle was refilled with ethanol and weighed as M_2. Then, GelMA samples were taken out, and the remaining bottle was measured as M_3. The porosities of lyophilized GelMA hydrogels were calculated according to the following formula:

$$\text{Porosity } (\%) = [(M_2-M_3-M_S)/(M_1-M_3)] \times 100\% \quad (1)$$

2.7.4 Swelling behavior

To determine the swelling behavior, lyophilized GelMA samples were measured as M_S. Subsequently, dried GelMA samples were immersed in PBS (0.01 M, pH7.4) for 24 h at 37℃. At each predetermined timepoint, GelMA hydrogels were taken out, and excess PBS was removed. The weight of swollen GelMA hydrogels was measured as M_S'. The swelling ratio of GelMA hydrogels was calculated according to the following formula:

$$\text{Swelling ratio } (\%) = [(M_S'-M_S)/M_S] \times 100\% \quad (2)$$

2.7.5 Mechanical properties

Mechanical properties of GelMA hydrogels were evaluated via compression tests.

Dried cylindrical GelMA samples (Φ10 × 5 mm) were used and compressed at a speed of 0.5 mm/min using a universal mechanical testing machine (Model 5848, Instron Ltd., USA). The ultimate compression strength of GelMA hydrogels was set as the highest load attained divided by the original cross-sectional area of the GelMA sample. The compression modulus was determined by the slope of the initial linear range of the compressive stress-strain curve.

2.8 *In vitro* biological performance of GelMA hydrogels

Bone marrow-derived mesenchymal stem cells (BMSCs) derived from adult rats in passage 3-8 were used to evaluate the *in vitro* biological behavior of GelMA hydrogels. Before cell culture, dried GelMA hydrogels were sterilized by gamma radiation and then soaked at PBS for 24h. BMSCs at a density of 5×10^3 cells per well were seeded on GelMA hydrogels (one sample per well in a 48-well plate). After attached for 1h, cell medium was added and hydrogels were cultured in the DMEM at 37℃ in a CO_2 incubator for 24h and 48h, respectively. The live/dead assay kit was employed to evaluate the survival rate of BMSCs cultured on the GelMA hydrogels. Living cells were stained green and dead cells were stained red under fluorescence microscope observation. On the other hand, to investigate the cell proliferation behavior, BMSCs at a density of 1×10^3 cells per well were seeded on GelMA hydrogels and cultured in DMEM for 1, 3, and 7 days. The cell viability was conducted using MTT tests.

2.9 Application of GelMA in 3D bioprinting

GelMA is a popular biomaterial for 3D bioprinting to construct cell-laden hydrogel structures. Given the gel-sol transition temperature and photocurable efficiency of

GelMA synthesized in the current study, a GelMA-PH solution was prepared for bioink formulation to show the application of GelMA in 3D bioprinting. GelMA-PH (5.0 wt.%) solution was mixed with a BMSCs suspension to make the bioink at the concentration of 1×10^6 BMSCs/ml. The hybrid bioink was installed on the 3D bioprinter (regenHU, Switzerland). The printing temperature was set at 20℃. Nozzle diameter was 0.4mm and the printing speed was set to match the inks extrusion rate. The BMSCs-laden GelMA-PH hydrogel was printed on the platform with 120s UV irradiation. After photo-crosslinking, cell-laden GelMA-PH hydrogel was transferred to a 6-well cell culture plate and cultured in DMEM at 37℃ in a CO_2 incubator. The survival rate of BMSCs in the printed GelMA-PH hydrogel was determined using live/dead assay kit.

2.10 Statistical analysis

The results presented in this article were obtained from at least 3 separate experiments and are expressed as the mean ± SD. The one-way ANOVA was performed for statistical analysis. Statistically significant difference existed when: *$p < 0.05$, **$p < 0.01$.

3. Results and discussion

3.1 Characterization of GelMA

In the current study, as shown in Fig.1A, four sets of GelMA samples were synthesized in PBS and CBS reaction systems. The exact reaction parameters for GelMA synthesis are listed in Table.1. To better explore the properties of GelMA synthesized in PBS and CBS, we controlled the GelMA DS at a high level (~80%) and a low level (~20%). Taking phenylalanine peaks (7.1-7.4 ppm) as the standard, the ^{1}H-NMR spectra in Fig.1B indicated that new peaks around 6.00–5.86 ppm (m, -O-CH_2-CH=CH_2) and 5.38–5.22 ppm (t, -OCH_2-CH=CH_2) appeared in GelMA chains. Also, the methyl peak at around 1.8 ppm and lysine methylene peak at 2.8-3.0 ppm demonstrated the successful methacryloylation of gelatin. Moreover, the quantitative results of DS were calculated via the TNBS method. Fig.1C showed that the DS of GelMA-PH, GelMA-PL, GelMA-CH, and GelMA-CL was 82.29±3.68, 20.23±5.99, 81.87±4.41, and 21.01±7.32%, respectively. As a result, GelMA-PH exhibited a similar DS (~80%) to GelMA-CH, and GelMA-PL had a comparative DS (~20%) to GelMA-CL. Previous studies have pointed out that CBS was superior to PBS for GelMA synthesis in terms of rendering free amino groups reactive via deprotonation and buffer capacity [28, 39], which led to high efficiency for GelMA synthesis under the CBS reaction system. The reason for this is that the GelMA synthesis reaction by-product, methacrylic acid (MA), could lower the solution pH, which would cause the free amino groups in gelatin ionized and further inhibit the reaction. Therefore, a high pH environment would improve the efficiency in GelMA synthesis. As depicted in Table.1, GelMA synthesized

261 in CBS indeed consumed less amount of MA. Moreover, due to the higher pH than PBS,
262 CBS at pH 9.0 enabled quick neutralization of MA as well as the formed methacrylate
263 groups through hydrolysis, thus resulting in the production of homogeneously reacted
264 GelMA [40].
265 Gelatin exhibits the partial triple-helix structure at gel status in low temperature while
266 forming the random coil structure at sol state upon heating. To investigate the effect of
267 methacryloylation on GelMA's physical structure, XRD analysis was conducted. As
268 shown in Fig.1D, gelatin displayed a peak around 20.5°, which was associated with the
269 triple helix structure [41, 42]. However, the functionalization of methacrylate groups in
270 gelatin chains might potentially interfere with the triple helix structure, thus resulting
271 in lower peak intensity at around 20.5°. The higher DS of GelMA, the lower peak
272 intensity. Additionally, the peak intensity of GelMA-PH was higher than GelMA-CH,
273 which illustrated that the triple helix structure of GelMA synthesized in CBS might be
274 dramatically damaged. It was speculated that the introduction of methacrylate groups
275 in gelatin chains could interfere with intrachain and interchain interaction, such as
276 hydrogen bonding, in the triple helix structure, causing the increase of the random coil
277 region and the decrease of triple helix formation [24]. Considering that the transition from
278 triple helix to random coil structure is reversible and associated with temperature,
279 GelMA with high DS and interference of triple helix structure would be less
280 temperature-sensitive. Consequently, the phase transition of GelMA-PH or GelMA-CH
281 (helix-random coil transition) could happen at a lower temperature than GelMA-PL or
282 GelMA-CL. On the other hand, GelMA-PH would exhibit a higher temperature phase

transition compared with GelMA-CH. Furthermore, the difference in the physical structure of GelMA would significantly influence the properties of resulting hydrogels, such as gel-sol transition temperature, photocurable efficiency, microstructure, swelling ratio, mechanical strength, and biological performance. The FT-IR spectra shown in Fig.1E indicated that all samples displayed the characteristic bands of the gelatin backbone: Amide I, Amide II, and Amide III [43].

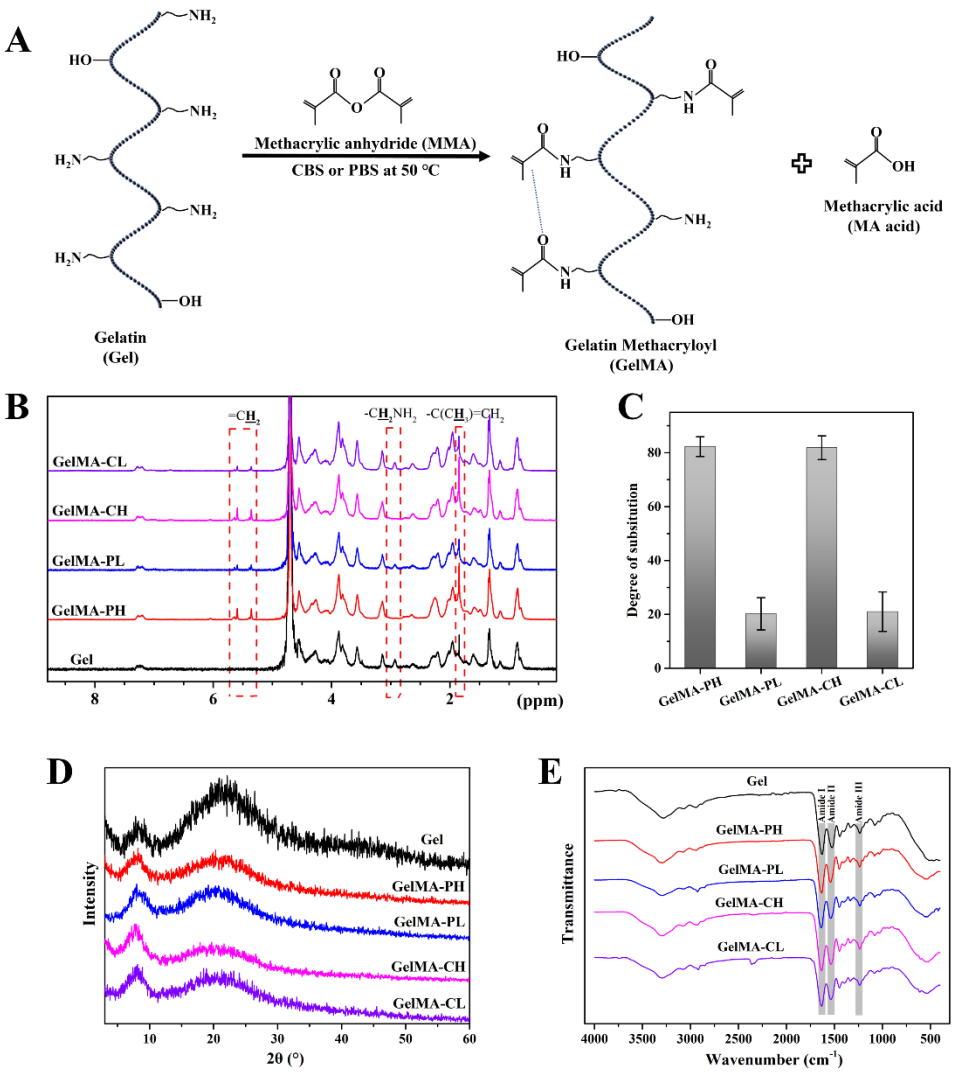

Fig.1 (A) A schematic illustration for GelMA synthesis. (B) ^{1}H-NMR spectra of Gel, GelMA-PH, GelMA-PL, GelMA-CH, and GelMA-CL. (C) Degree of

substitution of GelMA as calculated using the TNBS method. (D) XRD and (E) FT-IR spectra of Gel, GelMA-PH, GelMA-PL, GelMA-CH, and GelMA-CL.

Table.1 Reaction parameters for the synthesis of GelMA-PH, GelMA-PL, GelMA-CH, and GelMA-CL.

GelMA	Gelatin (g)	MA (ml)	CBS (ml)	PBS (ml)	T* (℃)	Time# (h)	Initial pH
GelMA-PH	10	8.0	0	100	60	1.0	7.4
GelMA-PL	10	0.8	0	100	60	1.0	7.4
GelMA-CH	10	1.0	100	0	60	1.0	9.0
GelMA-CL	10	0.2	100	0	60	1.0	9.0

T*: reaction temperature; Time#: reaction time.

3.2 Phase transition temperature of GelMA

For GelMA, it is essential to determine the phase transition temperature for the screening and selection of proper biomaterials for targeting biomedical applications [44, 45]. For example, GelMA, like gelatin, is a promising biomaterial for 3D printing because of its temperature sensitivity and good printability [46-48]. In this study, to ascertain the phase transition temperature of GelMA, a temperature sweep test was conducted. As shown in Fig.2A, the phase transition temperature of Gel, GelMA-PH, GelMA-PL, and GelMA-CL was 34.05℃, 30.96℃, 27.81℃, and 15.34℃, respectively. The sol-gel transition for GelMA-CH was unable to happen even at 4℃. Fig.2B illustrated that the viscosity of Gel, GelMA-PH, GelMA-PL, and GelMA-CL solutions dramatically

decreased at the temperature of 32.96℃, 30.82℃, 23.59℃, and 15.24℃, respectively, while GelMA-CH was constantly in solution state. Moreover, the optical images in Fig.2C showed that GelMA-CH was in the solution state at 4℃ and GelMA-CL was aqueous at 20℃. These results indicated that the physical structure of GelMA was less pronounced when gelatin was functionalized by methacrylate groups that might interfere with helix formation [15]. Furthermore, GelMA-PH and GelMA-PL presented high gel-sol transition temperatures compared to GelMA-CH and GelMA-CL. It meant that GelMA-PH and GelMA-PL possessed more triple helix formation, which was consistent with the XRD results (Fig.1D). Glycine-Proline-Hydroxyproline tripeptides are more likely to be responsible for triple helix structure formation [49]. Hydroxyl groups of hydroxyproline enables the reaction with MA in the alkaline environment and a high feed of MA [33]. The intervention of additional groups could influence triple helix formation. As a result, GelMA synthesized under the CBS reaction system exhibited decreased triple helix formation, which was demonstrated by the decreased phase transition temperature compared to GelMA prepared using PBS.

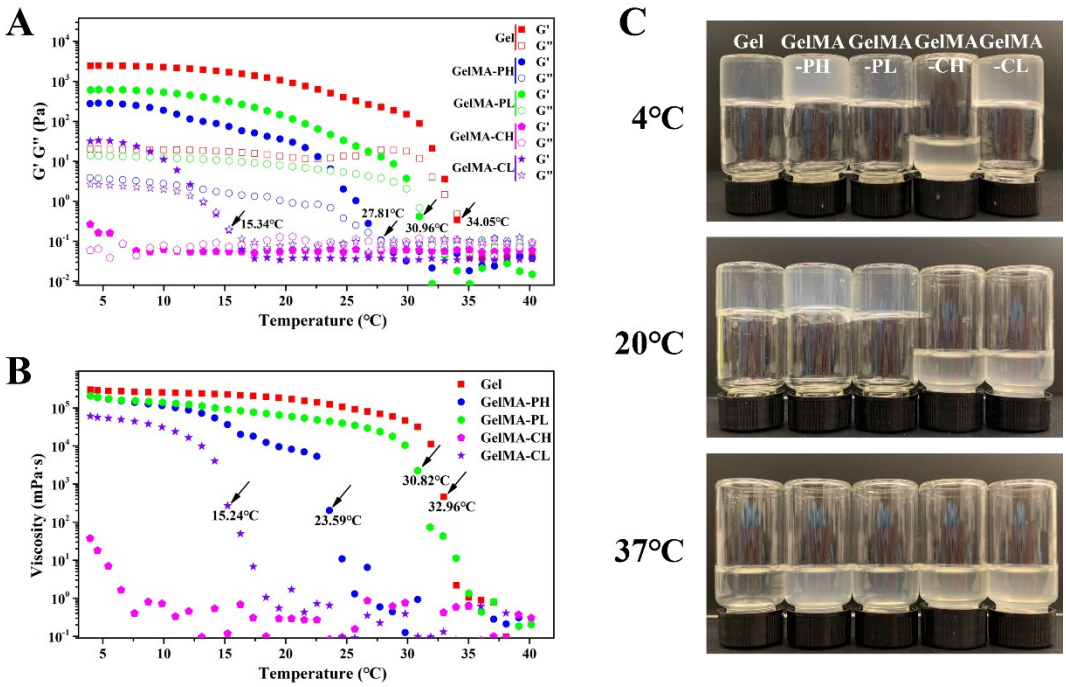

Fig.2 Variation of (A) G' and G" and (B) Viscosity in terms of temperature for Gel, GelMA-PH, GelMA-PL, GelMA-CH, and GelMA-CL. (C) Photos of Gel, GelMA-PH, GelMA-PL, GelMA-CH, and GelMA-CL in reversed bottles at different temperatures (4°C, 20°C, and 37°C).

3.3 Secondary structure of GelMA

It is well-known that gelatin exhibits temperature sensitivity, forming solid-state hydrogel at low temperatures because of partial triple helix structure formation and becoming aqueous solution upon heating due to random coil structure formation [50, 51]. The transition from triple helix to random coil is reversible. Although the phase transition study presented in Section 3.2 has shown that the methacryloylation of GelMA might interfere physical structure and therefore affect phase transition temperature and result in the decreased gel-sol phase transition temperature, GelMAs

synthesized in PBS or CBS were expected to retain a certain degree of the secondary structure of gelatin. To further investigate the differences in physical structure amongst GelMAs, the secondary structure of GelMAs synthesized in PBS and CBS, respectively, was analyzed using CD spectroscopy. Fig.3 displays CD spectra of Gel and GelMAs at 4℃, 20℃, and 37℃, respectively. As shown in Fig.3, the intensity at 198nm is ascribed to the random coil formation while the intensity at 222nm arises from the triple helix structure. Gelatin exhibited a much higher intensity at 222nm at 4℃ and 20℃ than GelMAs, which suggested that the functionalization of methacrylate groups in gelatin side chains would affect the secondary structure of gelatin (Table.S1) and hence reduce triple helix structure formation. Consequently, GelMAs had lower gel-sol transition temperatures than gelatin (Fig.2). On the other hand, GelMA-CH and GelMA-CL showed small rises at 199nm at 4℃ and 20℃ in comparison with GelMA-PH and GelMA-PL. The CD spectra indicated that the triple-helix contents of GelMA-CH and GelMA-CL at 222nm at 4℃ and 20℃ decreased significantly, as compared with GelMA-PH and GelMA-PL, suggesting that GelMA synthesized in PBS could retain a larger amount of triple-helix formation than GelMA in CBS. Additionally, GelMA-PL had a higher tensity at 222nm at 4℃ and 20℃, respectively, than GelMA-PH, indicating that lower methacryloylation of GelMA could retain a larger amount of triple-helix formation. As a result, GelMA with a low DS exhibited high temperature sensitivity, and its helix-random coil transition temperature would be higher. Moreover, Gel and GelMAs exhibited a large increase in intensity at 198nm at 37℃, as compared to those at 4℃ and 20℃, which suggested that Gel and GelMAs experienced a helix-

coil transition upon heating. Moreover, as can be observed by comparing Fig.3 here with Fig.S3 in Supporting Information, the intensity of gelatin under the CBS reaction system without the addition of MA at 222 nm was 2.37 and 0.73 at 4℃ and 20℃, respectively. Additionally, the intensity of gelatin under the PBS reaction system without the addition of MA at 222 nm was 2.11 at 4℃, suggested that the CBS and PBS reaction systems had little effect on triple helix formation.

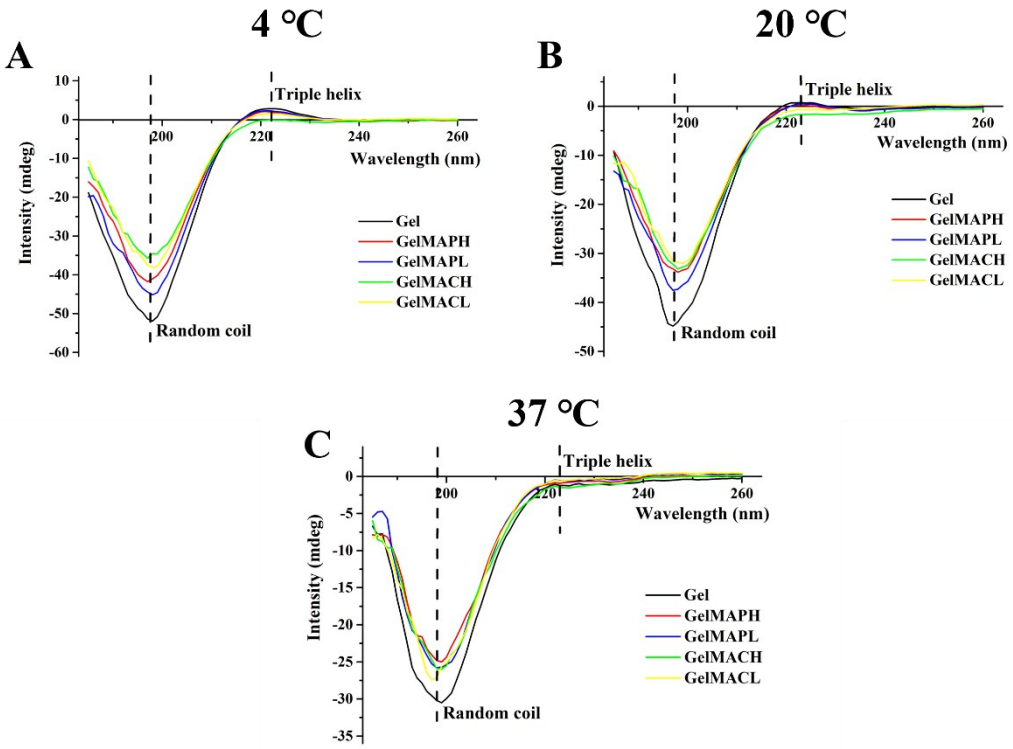

Fig.3 CD spectra of Gel, GelMA-PH, GelMA-PL, GelMA-CH, and GelMA-CL in DI water at a concentration of 0.2mg/ml at (A) 4℃, (B) 20℃, and (C) 37℃, respectively.

3.4 Characterization of GelMA hydrogels

In addition to the physical structure, the photocurable properties of GelMA are crucial for biomedical applications [52, 53]. Once GelMA is crosslinked in the presence of a photoinitiator, covalent bonding between the adjacent methacrylate groups forms, leading to the entanglement of the polypeptide chains and irreversible crosslinking, which endows the wide application of GelMA in 3D bioprinting to construct biomimetic tissues and organs for tissue engineering [54, 55]. It is known that GelMA synthesized from different methods exhibits distinct secondary structures and thus performs characteristic photocurable efficiency. The photocurable efficiency and process conditions, such as UV intensity, solution concentration, etc., govern the hydrogel formation, ultimately affecting the structural, mechanical, and biological characteristics of the resultant hydrogels [50, 56]. Herein, to investigate the photocurable efficiency of GelMA synthesized under PBS and CBS systems, 5.0% w/v GelMA and 0.5% v/v photoinitiator were co-dissolved to prepared GelMA hydrogels under UV exposure with different time (0s, 60s, 120s, 240s, and 480s). As shown in Fig.4A, the G' of GelMA-PH and GelMA-PL were much higher than G", which signified that GelMA-PH and GelMA-PL were in gel state at 20℃, while GelMA-CH and GelMA-CL were in sol state. Importantly, due to the high gel-sol transition temperature of GelMA-PL, GelMA-PL had the highest elastic modulus. When GelMA solutions were crosslinked by UV light to trigger free radical chain reaction polymerization, GelMA hydrogels formed (Fig.4B). GelMA-PH could quickly form the hydrogel when exposed to 365nm UV light for 60s. At the same time, GelMA-CH and GelMA-CL were unable to be crosslinked. Although GelMA-PL was in the gel state under 60s UV exposure, the slight increase of G' showed that

GelMA-PL had not been crosslinked (Fig.4C). As the increase of UV exposure time to 120s, GelMA-CH hydrogel began to form, and the G' of GelMA-PH exceeded GelMA-PL. GelMA-CL formed stable hydrogel when UV crosslink time reached 480s.

In consequence, it could be rationally speculated that GelMA synthesized in PBS exhibited higher photocurable efficiency than GelMA prepared in CBS. The difference of photocurable efficiency between GelMA sets might be attributed to the physical structure. Because the phase transition temperature of GelMA-PH and GelMA-PL are above 20℃, GelMA-PH and GelMA-PL are in the gel state, whereas GelMA-CH and GelMA-CL are aqueous at room temperature. Since GelMA-PH and GelMA-PL were in the thermally crosslinked state, which resulted in the compact structure, the interaction between neighboring methacrylate groups seemed to appear easily as compared with the loose structure of liquid GelMA-CH and GelMA-CL solutions. As a result, GelMA-PH and GelMA-PL had higher photocrosslinking efficiency. The higher photo-crosslinking efficiency, the less UV exposure time. Generally, cell-laden GelMA hydrogels are usually crosslinked by UV light. Unfortunately, UV light is harmful to cells and can cause cell apoptosis by inducing DNA fragmentation and protein maturation [57]. Therefore, it is critical to use those sets of GelMA with high photocurable efficiency for 3D bioprinting applications to reduce the UV radiation time and prevent the encapsulated cells from potential damage [58].

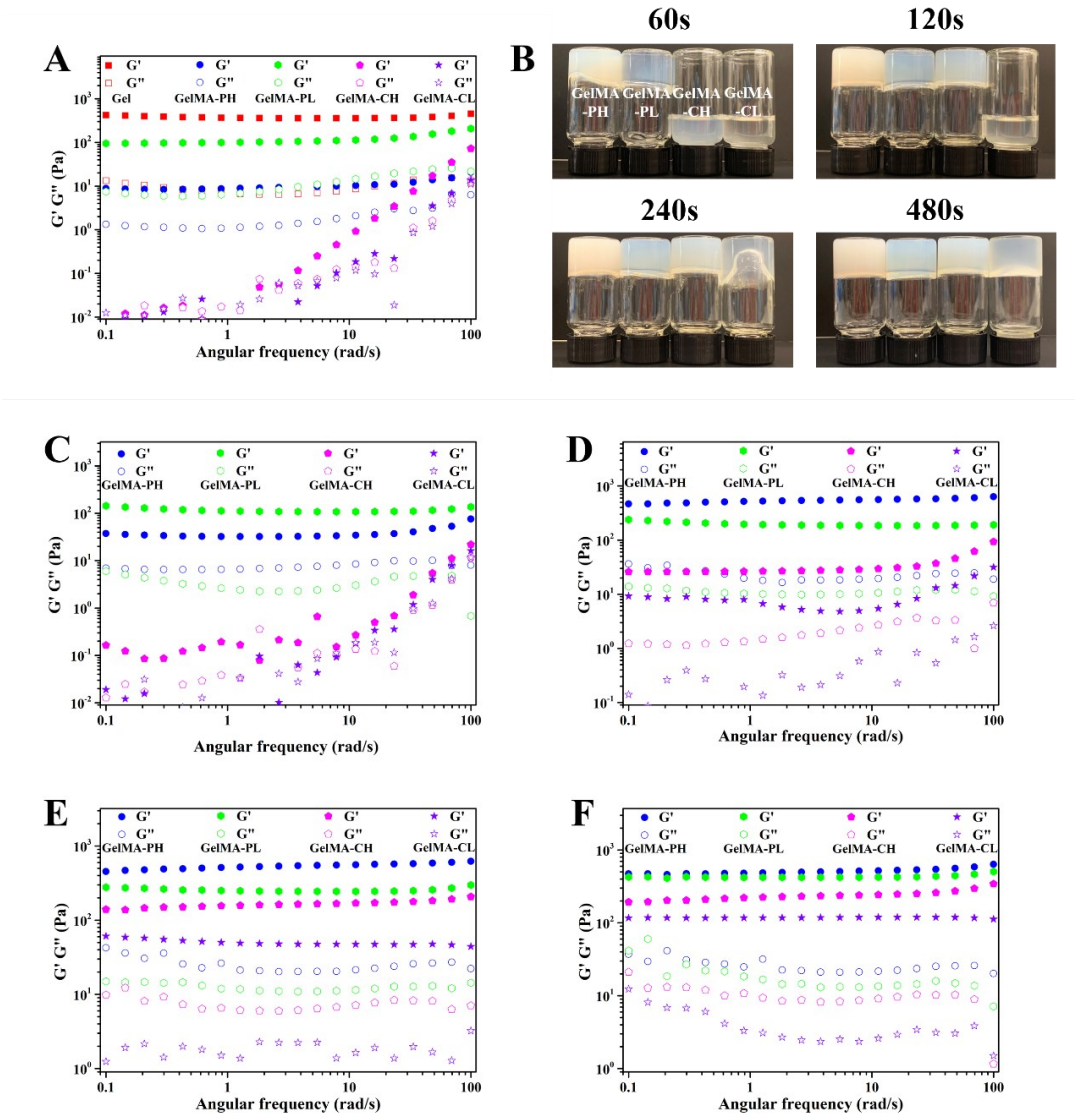

Fig.4 (A) Variation of G' and G" in terms of angular frequency for Gel, GelMA-PH, GelMA-PL, GelMA-CH, and GelMA-CL hydrogels without UV exposure. (B) Photos of Gel, GelMA-PH, GelMA-PL, GelMA-CH, and GelMA-CL hydrogels crosslinked by 365nm UV light for 60s, 120s, 240s, and 480s, respectively. Variation of G' and G" in terms of angular frequency for Gel, GelMA-PH, GelMA-PL, GelMA-CH, and GelMA-CL hydrogels crosslinked by UV light for (C) 60s, (D) 120s, (E) 240s, and (F) 480s.

Fig.5(A) displays the representative SEM images highlighting the microstructure of different GelMA hydrogel groups. The surface pore size and pore area percent calculated via Image J software are shown in Fig.5(B, C). Moreover, the pore size distribution of different GelMA hydrogel samples is presented in Fig.S2. It could be noted that both pore size and pore area percent were significantly affected by the UV exposure duration. The porosities of GelMA hydrogel samples measured via the Archimedes principle also demonstrated the effect of UV radiation time on GelMA microstructure (Fig.6). With the increase of UV exposure duration, which induced tighter entanglement of polypeptide network, the pore size, pore area percent, and porosity dramatically decreased. Additionally, GelMA synthesized in the same system (whether PBS or CBS) with high DS exhibited smaller pore size, pore area percent, and porosity than those with low DS. In this context, GelMA-PH and GelMA-CH hydrogels with high DS provided more reactive sites or methacrylate groups to trigger free radical chain reaction polymerization, thereby leading to a tight hydrogel network [30]. On the other hand, GelMA-CH samples had larger pore size, pore area percent, and porosity in comparison to GelMA synthesized in PBS, which indicated that the polypeptide network in GelMA-CH samples was less entangled. It could result from the difference in the physical structure of GelMA synthesized in PBS and CBS. Pore size and porosity play an essential role in nutrient and oxygen diffusion and waste removal, thereby affecting cell behaviors, including cell attachment, migration, proliferation, and differentiation [59]. Different pore sizes might induce different cell processes. Nano-sized pores are essential for collagen and extracellular matrix (ECM) formation, while micro-

sized pores are necessary for cell proliferation, differentiation, and cell-cell interaction. Previous studies have shown that scaffolds with 100-500μm pores were beneficial for bone regeneration [60]. In this study, when the UV exposure duration was beyond 120s, GelMA hydrogels possessed a relatively high modulus (Fig.4) and small pore size, which would impair biological properties.

The swelling behavior of hydrogels is an important feature for the diffusion manner of small molecules, such as nutrients and waste, in drug delivery and cell culture. Consequently, the swelling behavior of hydrogels would affect cell survival, growth, and tissue regeneration. Fig.7 indicates the swell performance of GelMA hydrogels after being cultured in PBS at 37℃ for 24h. Since GelMA-CH and GelMA-CL cannot form hydrogels without enough UV exposure time, some data is excluded. The swelling ratios of different GelMA sets crosslinked by different UV duration ranged from 450% to 1300%, which was consistent with previous studies [23, 33]. Theoretically, the UV exposure time, degree of substitution, and synthesis methods have a significant effect on the swelling ratio of GelMA hydrogels. The swelling ratio of GelMA hydrogels decreased with the increase of UV irradiation duration. GelMA hydrogels with high DS exhibited a lower swelling ratio. Moreover, GelMA hydrogels synthesized in CBS performed a higher swelling ratio because of the less entangled network compared with those prepared in PBS. Since GelMA-CH and GelMA-CL had higher swelling ratios and less entangled networks, which can lead to encapsulated or grafted drugs being quick released, GelMA-CH and GelMA-CL have potential applications for controlled quick drug release, such as anti-cancer drug delivery systems.

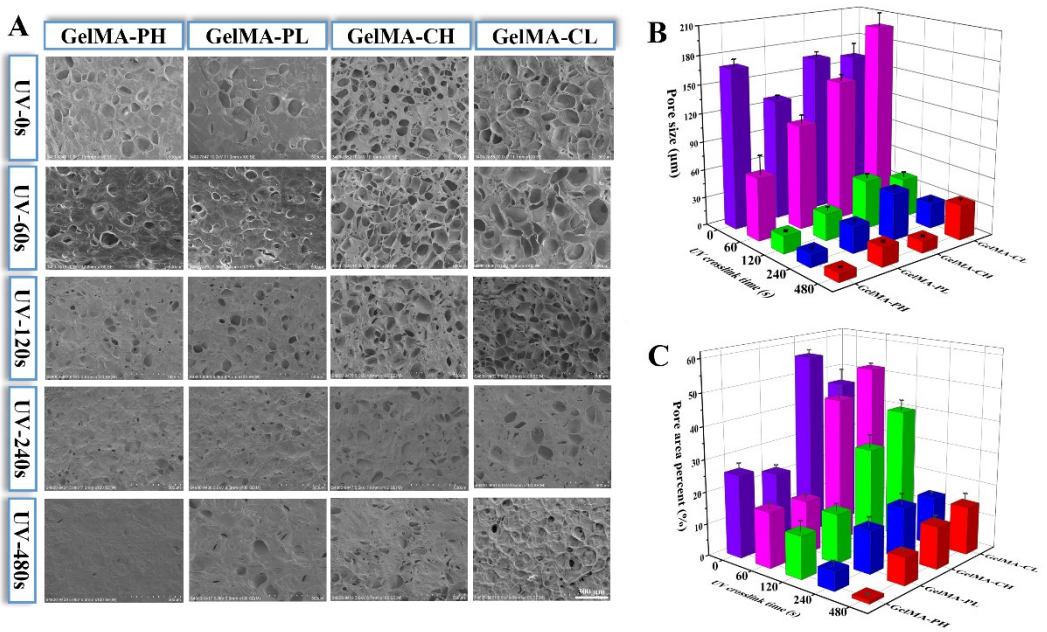

Fig.5 (A) SEM images of the surface morphology of Gel, GelMA-PH, GelMA-PL, GelMA-CH, and GelMA-CL hydrogels crosslinked by UV light for 0s, 60s, 120s, 240s, and 480s, respectively. (B) Pore size and (C) Pore area percentage of Gel, GelMA-PH, GelMA-PL, GelMA-CH, and GelMA-CL hydrogels crosslinked by UV light for 0s, 60s, 120s, 240s, and 480s, respectively.

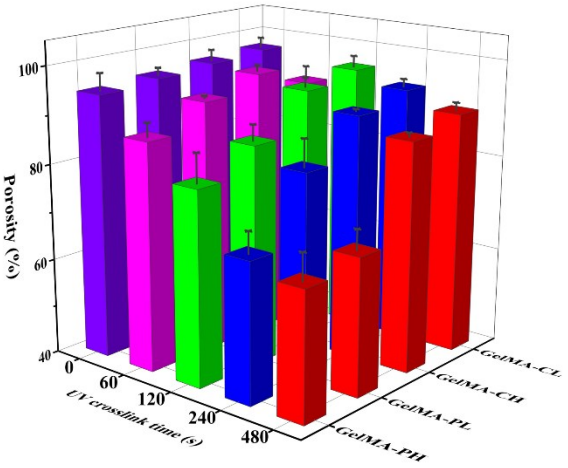

Fig.6 Porosity of Gel, GelMA-PH, GelMA-PL, GelMA-CH, and GelMA-CL

hydrogels crosslinked by UV light for 0s, 60s, 120s, 240s, and 480s, respectively.

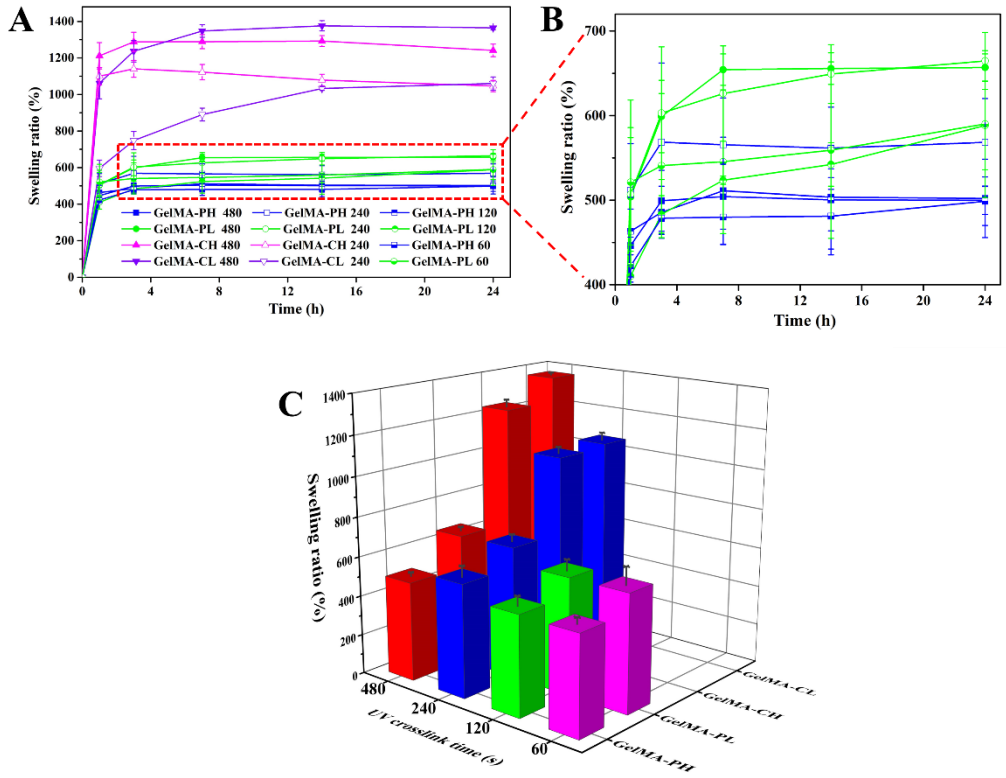

Fig.7 (A) and (B) Swelling behaviors of Gel, GelMA-PH, GelMA-PL, GelMA-CH, and GelMA-CL hydrogels. (C) Swelling ratios of Gel, GelMA-PH, GelMA-PL, GelMA-CH, and GelMA-CL hydrogels.

The mechanical properties of GelMA hydrogels crosslinked by different UV duration were investigated via compression test using a universal mechanical testing machine. As shown in Fig.8, among the GelMA hydrogels without UV crosslinking, GelMA-PL hydrogel exhibited the highest mechanical strength (0.169±0.017 MPa) and compression modulus (0.505±0.069 MPa). Perhaps, it could be due to the high phase

493 transition temperature of GelMA-PL. Compared with other GelMA hydrogels, the
494 physical structure of GelMA-PL was less likely to be disrupted by methacrylate groups
495 and thus preserved a similar secondary structure with gelatin. Therefore, GelMA-PL
496 hydrogel could have a more entangled network, which made the hydrogel robust. The
497 mechanical properties of GelMA hydrogels were significantly affected by UV crosslink
498 time [50, 61]. When GelMA hydrogels were exposed to UV irradiation, the mechanical
499 strength of GelMA-PH hydrogels dramatically increased and was the highest among
500 those hydrogels. The compression strength of GelMA-PH exposed to UV irradiation
501 for 60s, 120s, 240s, and 480s was 0.161±0.003 MPa, 0.273±0.013 MPa, 0.339±0.045
502 MPa, and 0.383±0.049 MPa, respectively. Since GelMA-PH had a high DS around 80%,
503 it could provide more reaction sites to trigger the polymerization, thereby forming a
504 stiff hydrogel network under UV exposure. On the other hand, as we have explained
505 that GelMA synthesized in PBS exhibited high photocurable efficiency due to the more
506 entangled hydrogel network at room temperature, GelMA-PH and GelMA-PL
507 hydrogels could be efficiently crosslinked by UV light irradation and thus show better
508 mechanical performance in comparison to GelMA-CH and GelMA-CL hydrogels. For
509 GelMA-CH and GelMA-CL hydrogels, owing to the significant interference to
510 secondary structure of GelMA molecules, GelMA-CH exhibited the lowest phase
511 transition temperature. Therefore, before efficient UV crosslink time, the mechancical
512 strength of GelMA-CH was lower than GelMA-CL. When the UV crosslink time
513 prolonged, the mechanical strength of GelMA-CH hydrogel would be higher than that
514 of GelMA-CL hydrogel.

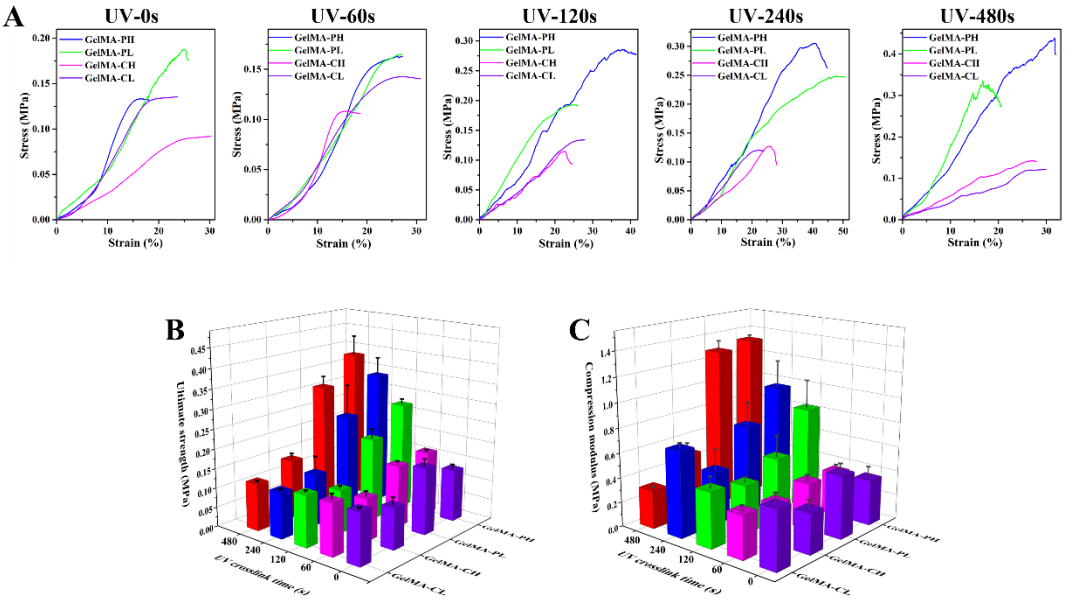

Fig.8 (A) Typical compressive stress-strain curves, (B) ultimate strength, and (C) compression modulus of GelMA-PH, GelMA-PL, GelMA-CH, and GelMA-CL hydrogels.

Since GelMA molecules synthesized in PBS and CBS, respectively, exhibited different physical structure and GelMA hydrogels prepared had distinct physiochemical properties, the biodegradation behavior of GelMA hydrogels and molecular chain length due to the hydrolysis would be different. Work on biodegradation of GelMAs for both GelMAs as raw materials and 3D printed GelMA structures is currently performed. The biodegradation results and new insights gained from comparative studies will be presented in a new publication.

3.5 *In vitro* biological properties of GelMA hydrogels

Cells are often seeded, encapsulated, or embedded in GelMA hydrogels to fabricate 3D scaffolds for tissue regeneration [62, 63]. It is crucial to evaluate the biological response of cells to those GelMA hydrogels. In this study, GelMA hydrogels crosslinked by UV

light for 480s were used to evaluate the biological properties. A high cell survival rate and cell viability yield were observed for all GelMA hydrogels. As shown in Fig.9A & B, GelMA hydrogels presented significantly high cell survival rates (over 90%) after being cultured for 24 h and 48h, which indicates that GelMA hydrogels are highly biocompatible. Notably, there was no significant difference among the cell survival rates in GelMA hydrogels. Fig.S4 shows the SEM images of cell morphology on the GelMA hydrogels surface after being cultured for 1d and 7d. Moreover, the cell proliferation behavior shown in Fig.9C indicated that GelMA-PH hydrogel exhibited the highest cell proliferation rate. Also, the proliferation rate of GelMA-PL hydrogel was higher than GelMA-CH and GelMA-CL hydrogels. This phenomenon could be explained by the mechanical strength differences. As mentioned, the mechanical strength of GelMA-PH and GelMA-PL hydrogels was higher than GelMA-CH and GelMA-CL hydrogels. Mechanical strength substantially affects cell behaviors [64, 65]. For example, the stress/strain of scaffolds could affect cell phenotypic change and functions, thereby promoting cell growth and differentiation.

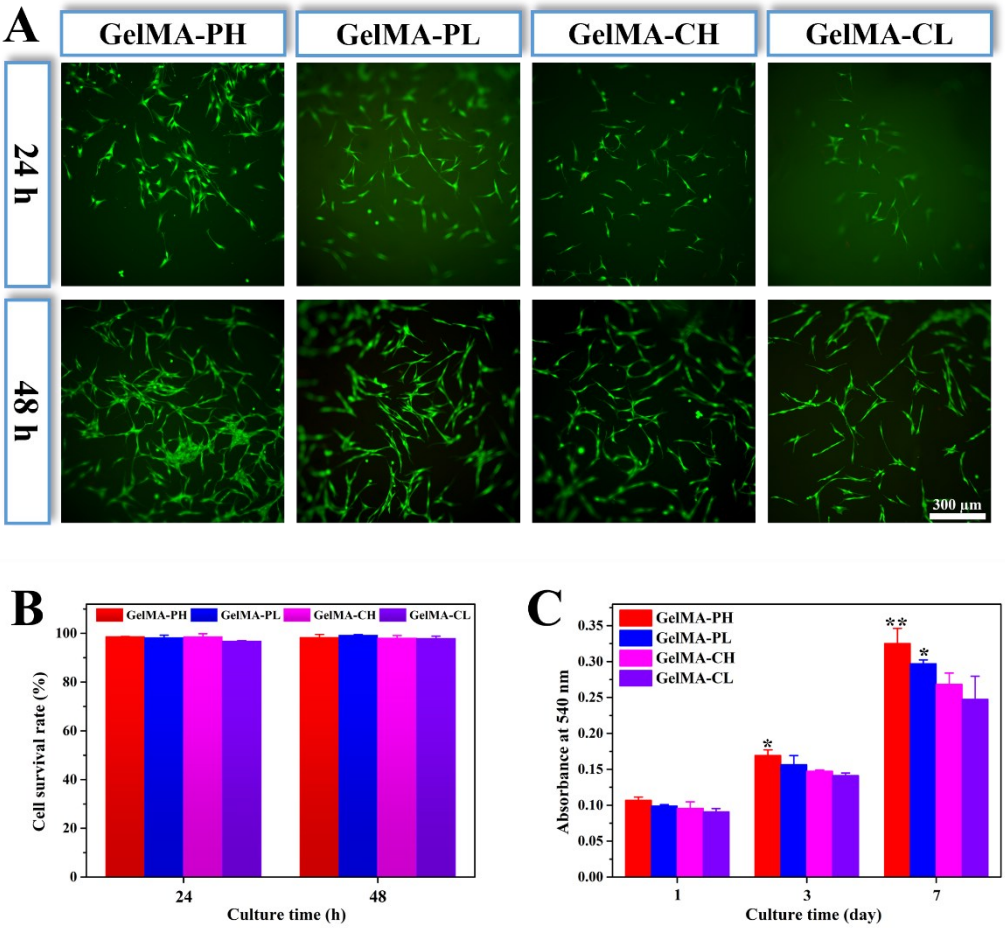

549

550 Fig.9 (A) Fluorescence images of GelMA-PH, GelMA-PL, GelMA-CH, and
551 GelMA-CL hydrogels after live (green) and dead (read) cell staining. (B) Cell
552 survival rate of BMSCs on the GelMA-PH, GelMA-PL, GelMA-CH, and
553 GelMA-CL hydrogels. (C) Cell proliferation behavior for GelMA-PH,
554 GelMA-PL, GelMA-CH, and GelMA-CL hydrogels.

555

556 3.6 Application of GelMA in 3D bioprinting

557 GelMA has been extensively used in 3D bioprinting due to its good biocompatibility,
558 thermo-reversible crosslinking, and chemical-irreversible crosslinking ability [35, 66]. In
559 the current study, considering the photocurable efficiency and gel-sol transition

560 temperature of synthesized GelMA, 5.0 wt.% GelMA-PH solution was mixed with
561 BMSCs suspension to fabricate bioink at a density of 1×10^6 cells/ml. A macroscopic
562 view of a 3D bioprinted GelMA-PH structure is shown as Fig.S5 in the Support
563 Information. As shown in Fig.10A, BMSCs were homogenously distributed in 3D
564 printed GelMA-PH hydrogel. Subsequently, BMSCs were stained using live/dead assay
565 to study the cell survival rate. Fig.10B and Fig.S6 indicated that BMSCs had a relatively
566 high survival rate (~95%) after 3D printing, which suggested that shear stress generated
567 during the 3D printing process did not impair the cell viability. Additionally, such a high
568 survival rate showed that 120s UV exposure has little effect on cell death. Although the
569 survival rate of BMSCs in 3D printed GelMA-PH hydrogel decreased to 86.3±4.1%
570 after cultured in DMEM for 1 day, survival rate recovered to 93.1±2.1% after 5-day
571 culture. On the other hand, GelMA-PH hydrogel could preserve stable structure after
572 5-day culture. Also, as the culture time increased, BMSCs tended to expand their
573 morphology in 3D printed GelMA-PH hydrogel (Fig.10C).
574

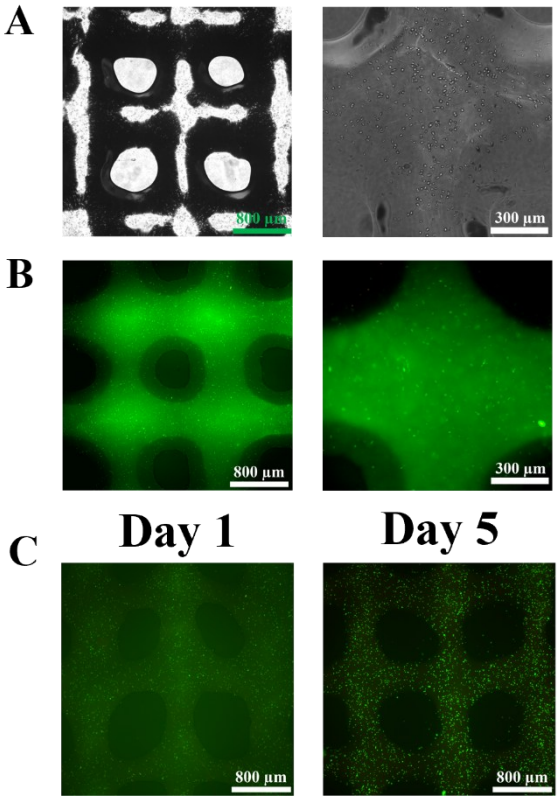

Fig.10 (A) Optical micrographs and (B) fluorescence images of BMSC-laden GelMA-PH hydrogel after 3D printing. (C) Fluorescence images of BMSC in 3D printed GelMA-PH hydrogel after cell culture for 1 and 5 days, respectively.

4. Conclusions

In this study, GelMA with two degrees of substitution (~20% and ~80%) has been synthesized under PBS and CBS reaction systems, respectively. Because the functionalization of methacrylate groups in the GelMA backbone would interfere with the intrachain and interchain interactions, GelMA synthesized in PBS exhibited distinct physical structures as compared with GelMA prepared in CBS. GelMA-PH and GelMA-PL hydrogels had higher phase transition temperature, photocurable efficiency, mechanical strength, and biological properties. In contrast, GelMA-CH and GelMA-CL hydrogels showed advantages in swelling performance and microstructure and possessed high porosity and large pore size. Additionally, BMSC-laden GelMA-PH hydrogel could be 3D printed and BMSCs exhibited relatively high survival rate in 3D printed hydrogel, showing the great potential of GelMA for 3D bioprinting. This focused study with systematic investigations has gained new insights into GelMA, which will provide guidance on the application of GelMA in 3D bioprinting and tissue engineering.

Author Contributions

Shangsi Chen: Conceptualization, Methodology, Investigation, Writing, Revision. **Yue Wang:** Methodology, Investigation, Writing, Revision. **Jiahui Lai**: Investigation, Writing. **Shenglong Tan:** Methodology, Investigation, Writing, Revision. **Min Wang:** Supervision, Writing, Editing, Reviewing, Revision.

Conflicts of interest

There are no conflicts to declare.

Supporting information

Glycine calibration curve; pore size distributions on surfaces of Gel and GelMA hydrogels; CD spectra of Gel under the CBS reaction system without the addition MA; SEM images of BMSCs morphology; macroscopic view of a 3D bioprinted GelMA-PH structure; survival rate of BMSCs in 3D bioprinted GelMA-PH hydrogel; CD spectra intensity (at 198nm and 222nm) of Gel, GelMA-PH, GelMA-PL, GelMA-CH, and GelMA-CL at 4℃, 20℃, and 37℃, respectively.

Acknowledgments

This work was financially supported by Hong Kong's Research Grants Council (RGC) through research grants (17200519, 17202921, 17201622 and N_HKU749/22) and National Nature Science Foundation of China (Grant No. 82201133). Shangsi Chen, Yue Wang and Jiahui Lai thank The University of Hong Kong (HKU) for providing them with PhD scholarships.

References

1. Bernhard, S.; Tibbitt, M. W., Supramolecular engineering of hydrogels for drug delivery. *Adv. Drug Delivery Rev.* **2021,** *171*, 240-256.
2. Mazidi, Z.; Javanmardi, S.; Naghib, S. M.; Mohammadpour, Z., Smart stimuli-responsive implantable drug delivery systems for programmed and on-demand cancer treatment: An overview on the emerging materials. *Chem Eng J* **2022,** *433*, 134569.
3. Zhao, Z.; Wang, Z.; Li, G.; Cai, Z.; Wu, J.; Wang, L.; Deng, L.; Cai, M.; Cui, W., Injectable microfluidic hydrogel microspheres for cell and drug delivery. *Adv. Funct. Mater.* **2021,** *31* (31), 2103339.
4. Sanchez-Cid, P.; Jimenez-Rosado, M.; Romero, A.; Perez-Puyana, V., Novel trends in hydrogel development for biomedical applications: a review. *Polymers* **2022,** *14* (15), 3023.
5. Alizadehgiashi, M.; Nemr, C. R.; Chekini, M.; Pinto Ramos, D.; Mittal, N.; Ahmed, S. U.; Khuu, N.; Kelley, S. O.; Kumacheva, E., Multifunctional 3D-printed wound dressings. *ACS Nano* **2021,** *15* (7), 12375-12387.
6. Bai, X.; Gao, M.; Syed, S.; Zhuang, J.; Xu, X.; Zhang, X. Q., Bioactive hydrogels for bone regeneration. *Bioact. Mater.* **2018,** *3* (4), 401-417.
7. Homaeigohar, S.; Tsai, T. Y.; Young, T. H.; Yang, H. J.; Ji, Y. R., An electroactive alginate hydrogel nanocomposite reinforced by functionalized graphite nanofilaments for neural tissue engineering. *Carbohydr. Polym.* **2019,** *224*, 115112.
8. Yang, D., Recent advances in hydrogels. *Chem. Mater.* **2022,** *34* (5), 1987-1989.
9. Li, Y.; Yang, H. Y.; Lee, D. S., Advances in biodegradable and injectable hydrogels for biomedical applications. *J. Controlled Release* **2021,** *330*, 151-160.
10. Yang, Y.; Campbell Ritchie, A.; Everitt, N. M., Recombinant human collagen/chitosan-based soft hydrogels as biomaterials for soft tissue engineering. *Mater. Sci. Eng., C* **2021,** *121*, 111846.
11. Farasatkia, A.; Kharaziha, M., Robust and double-layer micro-patterned bioadhesive based on silk nanofibril/GelMA-alginate for stroma tissue engineering. *Int. J. Biol. Macromol.* **2021,** *183*, 1013-1025.
12. Chen, S.; Wang, Y.; Zhang, X.; Ma, J.; Wang, M., Double-crosslinked bifunctional hydrogels with encapsulated anti-cancer drug for bone tumor cell ablation and bone tissue regeneration. *Colloids Surf., B* **2022,** *213*, 112364.
13. Kim, M. H.; Nguyen, H.; Chang, C. Y.; Lin, C. C., Dual functionalization of gelatin for orthogonal and dynamic hydrogel cross-linking. *ACS Biomater. Sci. Eng.* **2021,** *7* (9), 4196-4208.
14. Abudula, T.; Colombani, T.; Alade, T.; Bencherif, S. A.; Memic, A., Injectable lignin-co-gelatin cryogels with antioxidant and antibacterial properties for biomedical applications. *Biomacromolecules* **2021,** *22* (10), 4110-4121.
15. Yue, K.; Trujillo-de Santiago, G.; Alvarez, M. M.; Tamayol, A.; Annabi, N.; Khademhosseini, A., Synthesis, properties, and biomedical applications of gelatin methacryloyl (GelMA) hydrogels. *Biomaterials* **2015,** *73*, 254-71.
16. Li, Y.; Liu, C.; Cheng, X.; Zhang, A.; Liu, W.; Zhang, S.; Jian, X., Tunicate inspired gelatin-based tough hydrogel wound dressing containing twisted phthalazinone with adhesive, self-healing and antibacterial properties. *Int. J. Biol.*

Macromol. **2022,** *218*, 639-653.
17. Zou, S.; Fan, S.; Oliveira, A. L.; Yao, X.; Zhang, Y.; Shao, H., 3D printed gelatin scaffold with improved shape fidelity and cytocompatibility by using Antheraea pernyi silk fibroin nanofibers. *Adv. Fiber Mater.* **2022,** *4* (4), 758-773.
18. Li, J.; Zhang, Y.; Zhou, X.; Wang, S.; Hao, R.; Han, J.; Li, M.; Zhao, Y.; Chen, C.; Xu, H., Enzymatically functionalized RGD-gelatin scaffolds that recruit host mesenchymal stem cells in vivo and promote bone regeneration. *J. Colloid Interface Sci.* **2022,** *612*, 377-391.
19. Chen, S.; Shi, Y.; Zhang, X.; Ma, J., 3D printed hydroxyapatite composite scaffolds with enhanced mechanical properties. *Ceram. Int.* **2019,** *45* (8), 10991-10996.
20. Chen, S.; Shi, Y.; Zhang, X.; Ma, J., Evaluation of BMP-2 and VEGF loaded 3D printed hydroxyapatite composite scaffolds with enhanced osteogenic capacity in vitro and in vivo. *Mater. Sci. Eng., C* **2020,** *112*, 110893.
21. Bertlein, S.; Brown, G.; Lim, K. S.; Jungst, T.; Boeck, T.; Blunk, T.; Tessmar, J.; Hooper, G. J.; Woodfield, T. B. F.; Groll, J., Thiol-ene clickable gelatin: a platform bioink for multiple 3D biofabrication technologies. *Adv. Mater.* **2017,** *29* (44), 1703404.
22. Kreller, T.; Distler, T.; Heid, S.; Gerth, S.; Detsch, R.; Boccaccini, A. R., Physico-chemical modification of gelatine for the improvement of 3D printability of oxidized alginate-gelatine hydrogels towards cartilage tissue engineering. *Mater. Des.* **2021,** *208*, 109877.
23. Wang, Z.; Tian, Z.; Menard, F.; Kim, K., Comparative study of gelatin methacrylate hydrogels from different sources for biofabrication applications. *Biofabrication* **2017,** *9* (4), 044101.
24. An I. Van Den Bulcke; Bogdan Bogdanov; Nadine De Rooze; Etienne H. Schacht; Maria Cornelissen; Berghmans, H., Structural and rheological properties of methacrylamide modified gelatin hydrogels. *Biomacromolecules* **2000,** *1* (1), 31-38.
25. Man, K.; Barroso, I. A.; Brunet, M. Y.; Peacock, B.; Federici, A. S.; Hoey, D. A.; Cox, S. C., Controlled release of epigenetically-enhanced extracellular vesicles from a GelMA/nanoclay composite hydrogel to promote bone repair. *Int. J. Mol. Sci.* **2022,** *23* (2), 832.
26. Kurian, A. G.; Singh, R. K.; Patel, K. D.; Lee, J. H.; Kim, H. W., Multifunctional GelMA platforms with nanomaterials for advanced tissue therapeutics. *Bioact. Mater.* **2022,** *8*, 267-295.
27. Ribeiro, J. S.; Bordini, E. A. F.; Ferreira, J. A.; Mei, L.; Dubey, N.; Fenno, J. C.; Piva, E.; Lund, R. G.; Schwendeman, A.; Bottino, M. C., Injectable MMP-responsive nanotube-modified gelatin hydrogel for dental infection ablation. *ACS Appl. Mater. Interfaces* **2020,** *12* (14), 16006-16017.
28. Shirahama, H.; Lee, B. H.; Tan, L. P.; Cho, N. J., Precise tuning of facile one-pot gelatin methacryloyl (GelMA) synthesis. *Sci. Rep.* **2016,** *6*, 31036.
29. Young, A. T.; White, O. C.; Daniele, M. A., Rheological properties of coordinated physical gelation and chemical crosslinking in gelatin methacryloyl (GelMA) hydrogels. *Macromol. Biosci.* **2020,** *20* (12), e2000183.
30. Chansoria, P.; Asif, S.; Polkoff, K.; Chung, J.; Piedrahita, J. A.; Shirwaiker,

R. A., Characterizing the effects of synergistic thermal and photo-cross-linking during biofabrication on the structural and functional properties of gelatin methacryloyl (GelMA) hydrogels. *ACS Biomater. Sci. Eng.* **2021,** *7* (11), 5175-5188.
31. Hoch, E.; Hirth, T.; Tovar, G. E. M.; Borchers, K., Chemical tailoring of gelatin to adjust its chemical and physical properties for functional bioprinting. *J. Mater. Chem. B* **2013,** *1* (41), 5675-5685.
32. Lee, B. H.; Lum, N.; Seow, L. Y.; Lim, P. Q.; Tan, L. P., Synthesis and characterization of types A and B gelatin methacryloyl for bioink applications. *Materials* **2016,** *9* (10), 797.
33. Zhu, M.; Wang, Y.; Ferracci, G.; Zheng, J.; Cho, N. J.; Lee, B. H., Gelatin methacryloyl and its hydrogels with an exceptional degree of controllability and batch-to-batch consistency. *Sci. Rep.* **2019,** *9* (1), 6863.
34. Kumar, H.; Sakthivel, K.; Mohamed, M. G. A.; Boras, E.; Shin, S. R.; Kim, K., Designing gelatin methacryloyl (GelMA)-based bioinks for visible light stereolithographic 3D biofabrication. *Macromol. Biosci.* **2021,** *21* (1), e2000317.
35. Erdem, A.; Darabi, M. A.; Nasiri, R.; Sangabathuni, S.; Ertas, Y. N.; Alem, H.; Hosseini, V.; Shamloo, A.; Nasr, A. S.; Ahadian, S.; Dokmeci, M. R.; Khademhosseini, A.; Ashammakhi, N., 3D bioprinting of oxygenated cell-laden gelatin methacryloyl constructs. *Adv. Healthcare Mater.* **2020,** *9* (15), e1901794.
36. Ruberu, K.; Senadeera, M.; Rana, S.; Gupta, S.; Chung, J.; Yue, Z.; Venkatesh, S.; Wallace, G., Coupling machine learning with 3D bioprinting to fast track optimisation of extrusion printing. *Appl. Mater. Today* **2021,** *22*, 100914.
37. Nichol, J. W.; Koshy, S. T.; Bae, H.; Hwang, C. M.; Yamanlar, S.; Khademhosseini, A., Cell-laden microengineered gelatin methacrylate hydrogels. *Biomaterials* **2010,** *31* (21), 5536-44.
38. Kathuria, N.; Tripathi, A.; Kar, K. K.; Kumar, A., Synthesis and characterization of elastic and macroporous chitosan-gelatin cryogels for tissue engineering. *Acta Biomater.* **2009,** *5* (1), 406-18.
39. Lee, B. H.; Shirahama, H.; Cho, N.-J.; Tan, L. P., Efficient and controllable synthesis of highly substituted gelatin methacrylamide for mechanically stiff hydrogels. *RSC Adv.* **2015,** *5* (128), 106094-106097.
40. Zheng, J.; Zhu, M.; Ferracci, G.; Cho, N.-J.; Lee, B. H., Hydrolytic stability of methacrylamide and methacrylate in gelatin methacryloyl and decoupling of gelatin methacrylamide from gelatin methacryloyl through hydrolysis. *Macromol. Chem. Phys.* **2018,** *219* (18), 1800266.
41. Rizwan, M.; Peh, G. S. L.; Ang, H. P.; Lwin, N. C.; Adnan, K.; Mehta, J. S.; Tan, W. S.; Yim, E. K. F., Sequentially-crosslinked bioactive hydrogels as nano-patterned substrates with customizable stiffness and degradation for corneal tissue engineering applications. *Biomaterials* **2017,** *120*, 139-154.
42. Choi, Y. H.; Kim, S. H.; Kim, I. S.; Kim, K.; Kwon, S. K.; Hwang, N. S., Gelatin-based micro-hydrogel carrying genetically engineered human endothelial cells for neovascularization. *Acta Biomater.* **2019,** *95*, 285-296.
43. Leu Alexa, R.; Iovu, H.; Ghitman, J.; Serafim, A.; Stavarache, C.; Marin, M. M.; Ianchis, R., 3D-printed gelatin methacryloyl-based scaffolds with potential

application in tissue engineering. *Polymers (Basel)* **2021,** *13* (5), 727.
44. Gasek, N.; Weiss, D. J., Effect of temperature on gelation and cross-linking of gelatin methacryloyl for biomedical applications. *Phys. Fluids* **2020,** *32* (3), 033102.
45. Di Muzio, L.; Cienzo, F.; Paolicelli, P.; Petralito, S.; Garzoli, S.; Brandelli, C.; Trilli, J.; Antonietta Casadei, M., A convenient strategy to synthesize highly tunable gelatin methacryloyl with very low gelation temperature. *Eur. Polym. J.* **2021,** *154*, 110538.
46. Chen, S.; Shi, Y.; Zhang, X.; Ma, J., Biomimetic synthesis of Mg-substituted hydroxyapatite nanocomposites and three-dimensional printing of composite scaffolds for bone regeneration. *J. Biomed. Mater. Res., Part A* **2019,** *107* (11), 2512-2521.
47. Qiao, Z.; Lian, M.; Han, Y.; Sun, B.; Zhang, X.; Jiang, W.; Li, H.; Hao, Y.; Dai, K., Bioinspired stratified electrowritten fiber-reinforced hydrogel constructs with layer-specific induction capacity for functional osteochondral regeneration. *Biomaterials* **2021,** *266*, 120385.
48. Bertassoni, L. E.; Cardoso, J. C.; Manoharan, V.; Cristino, A. L.; Bhise, N. S.; Araujo, W. A.; Zorlutuna, P.; Vrana, N. E.; Ghaemmaghami, A. M.; Dokmeci, M. R.; Khademhosseini, A., Direct-write bioprinting of cell-laden methacrylated gelatin hydrogels. *Biofabrication* **2014,** *6* (2), 024105.
49. Motooka, D.; Kawahara, K.; Nakamura, S.; Doi, M.; Nishi, Y.; Nishiuchi, Y.; Kang, Y. K.; Nakazawa, T.; Uchiyama, S.; Yoshida, T.; Ohkubo, T.; Kobayashi, Y., The triple helical structure and stability of collagen model peptide with 4(S)-hydroxyprolyl-Pro-Gly units. *Biopolymers* **2012,** *98* (2), 111-21.
50. Schuurman, W.; Levett, P. A.; Pot, M. W.; van Weeren, P. R.; Dhert, W. J.; Hutmacher, D. W.; Melchels, F. P.; Klein, T. J.; Malda, J., Gelatin-methacrylamide hydrogels as potential biomaterials for fabrication of tissue-engineered cartilage constructs. *Macromol. Biosci.* **2013,** *13* (5), 551-61.
51. Rebers, L.; Reichsollner, R.; Regett, S.; Tovar, G. E. M.; Borchers, K.; Baudis, S.; Southan, A., Differentiation of physical and chemical cross-linking in gelatin methacryloyl hydrogels. *Sci. Rep.* **2021,** *11* (1), 3256.
52. Gan, D.; Xu, T.; Xing, W.; Wang, M.; Fang, J.; Wang, K.; Ge, X.; Chan, C. W.; Ren, F.; Tan, H.; Lu, X., Mussel-inspired dopamine oligomer intercalated tough and resilient gelatin methacryloyl (GelMA) hydrogels for cartilage regeneration. *J. Mater. Chem. B* **2019,** *7* (10), 1716-1725.
53. Ning, L.; Mehta, R.; Cao, C.; Theus, A.; Tomov, M.; Zhu, N.; Weeks, E. R.; Bauser-Heaton, H.; Serpooshan, V., Embedded 3D bioprinting of gelatin methacryloyl-based constructs with highly tunable structural fidelity. *ACS Appl. Mater. Interfaces* **2020,** *12* (40), 44563-44577.
54. Gockler, T.; Haase, S.; Kempter, X.; Pfister, R.; Maciel, B. R.; Grimm, A.; Molitor, T.; Willenbacher, N.; Schepers, U., Tuning superfast curing thiol-norbornene-functionalized gelatin hydrogels for 3D bioprinting. *Adv. Healthcare Mater.* **2021,** *10* (14), e2100206.
55. Li, Z.; Li, S.; Yang, J.; Ha, Y.; Zhang, Q.; Zhou, X.; He, C., 3D bioprinted gelatin/gellan gum-based scaffold with double-crosslinking network for vascularized bone regeneration. *Carbohydr. Polym.* **2022,** *290*, 119469.

56. O'Connell, C. D.; Zhang, B.; Onofrillo, C.; Duchi, S.; Blanchard, R.; Quigley, A.; Bourke, J.; Gambhir, S.; Kapsa, R.; Di Bella, C.; Choong, P.; Wallace, G. G., Tailoring the mechanical properties of gelatin methacryloyl hydrogels through manipulation of the photocrosslinking conditions. *Soft Matter* **2018,** *14* (11), 2142-2151.
57. Masuma, R.; Kashima, S.; Kurasaki, M.; Okuno, T., Effects of UV wavelength on cell damages caused by UV irradiation in PC12 cells. *J. Photochem. Photobiol., B* **2013,** *125*, 202-8.
58. Lim, K. S.; Abinzano, F.; Bernal, P. N.; Albillos Sanchez, A.; Atienza-Roca, P.; Otto, I. A.; Peiffer, Q. C.; Matsusaki, M.; Woodfield, T. B. F.; Malda, J.; Levato, R., One-step photoactivation of a dual-functionalized bioink as cell carrier and cartilage-binding glue for chondral regeneration. *Adv. Healthcare Mater.* **2020,** *9* (15), e1901792.
59. Bruzauskaite, I.; Bironaite, D.; Bagdonas, E.; Bernotiene, E., Scaffolds and cells for tissue regeneration: different scaffold pore sizes-different cell effects. *Cytotechnology* **2016,** *68* (3), 355-69.
60. Abbasi, N.; Hamlet, S.; Love, R. M.; Nguyen, N.-T., Porous scaffolds for bone regeneration. *J. Sci.: Adv. Mater. Devices* **2020,** *5* (1), 1-9.
61. Basara, G.; Yue, X.; Zorlutuna, P., Dual crosslinked gelatin methacryloyl hydrogels for photolithography and 3D printing. *Gels* **2019,** *5* (3), 34.
62. Yuan, Z.; Yuan, X.; Zhao, Y.; Cai, Q.; Wang, Y.; Luo, R.; Yu, S.; Wang, Y.; Han, J.; Ge, L.; Huang, J.; Xiong, C., Injectable GelMA cryogel microspheres for modularized cell delivery and potential vascularized bone regeneration. *Small* **2021,** *17* (11), e2006596.
63. Dai, W.; Zhang, L.; Yu, Y.; Yan, W.; Zhao, F.; Fan, Y.; Cao, C.; Cai, Q.; Hu, X.; Ao, Y., 3D bioprinting of heterogeneous constructs providing tissue-specific microenvironment based on host–guest modulated dynamic hydrogel bioink for osteochondral regeneration. *Adv. Funct. Mater.* **2022,** *32* (23), 2200710.
64. Baker, S. C.; Rohman, G.; Southgate, J.; Cameron, N. R., The relationship between the mechanical properties and cell behaviour on PLGA and PCL scaffolds for bladder tissue engineering. *Biomaterials* **2009,** *30* (7), 1321-8.
65. Wang, L.; Wang, C.; Wu, S.; Fan, Y.; Li, X., Influence of the mechanical properties of biomaterials on degradability, cell behaviors and signaling pathways: current progress and challenges. *Biomater. Sci.* **2020,** *8* (10), 2714-2733.
66. Galliger, Z.; Vogt, C. D.; Helms, H. R.; Panoskaltsis-Mortari, A., Extracellular matrix microparticles improve GelMA bioink resolution for 3D bioprinting at ambient temperature. *Macromol. Mater. Eng.* **2022,** *307* (10), 2200196.

Supporting Information

Structure and Properties of Gelatin Methacryloyl (GelMA) Synthesized in Different Reaction Systems

Shangsi Chen [a 1], Yue Wang [a 1], Jiahui Lai [a], Shenglong Tan [b, c, *], Min Wang [a, *]

[a] Department of Mechanical Engineering
The University of Hong Kong
Pokfulam Road, Hong Kong

[b] Department of Endodontics, Stomatological Hospital
Southern Medical University
Guangzhou, China

[c] School of Stomatology
Southern Medical University
Guangzhou, China

Keywords: GelMA synthesis, physical structure, photocurable efficiency, tissue engineering, 3D bioprinting

* Corresponding Authors:
Professor Min Wang, at the University of Hong Kong, Hong Kong, China
Email: memwang@hku.hk Tel: +852 3971 7903 Fax: +852 2858541
Dr. Shenglong Tan, at the Stomatological Hospital of Southern Medical University, Guangzhou, China
Email: tansl@hust.edu.cn
[1] These authors contributed equally to this work

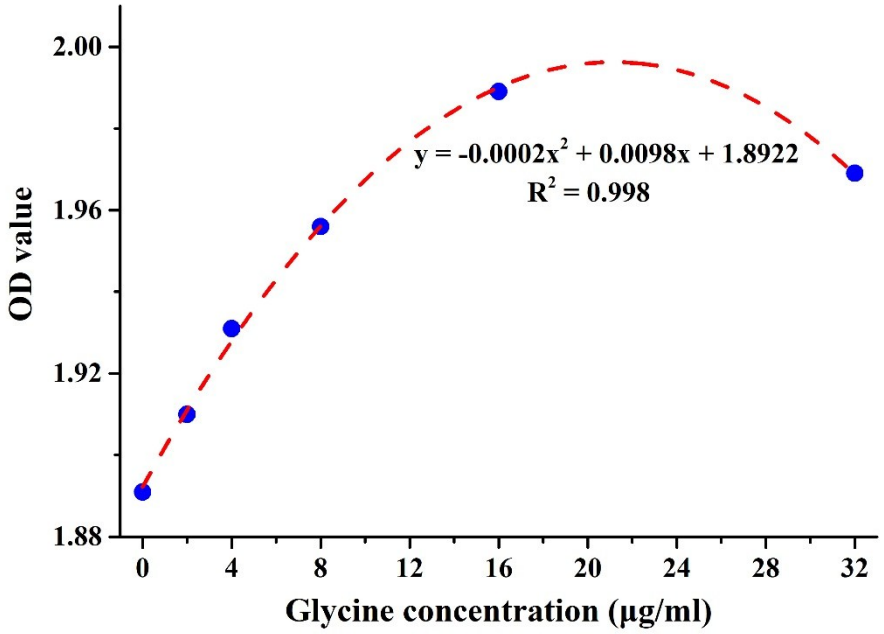

Fig.S1 Glycine calibration curve.

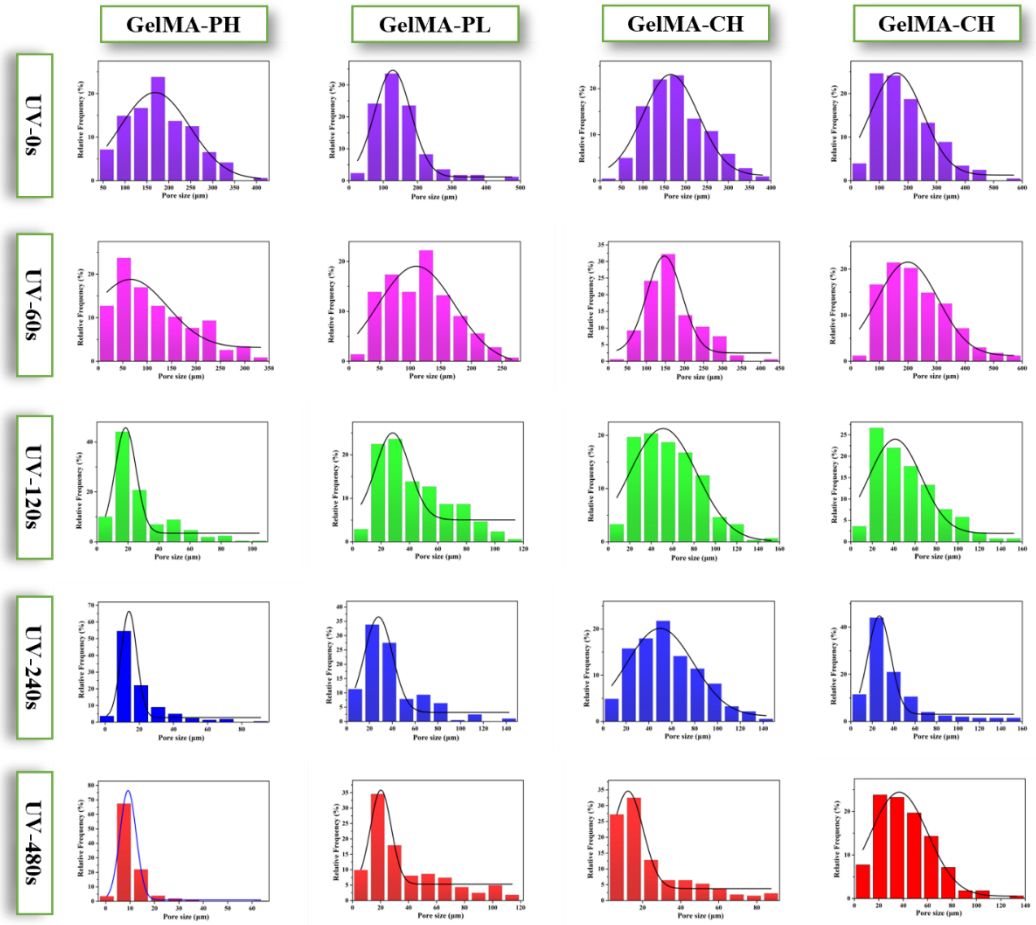

Fig.S2 Pore size distributions on surfaces of Gel, GelMA-PH, GelMA-PL, GelMA-CH, and GelMA-CL hydrogels crosslinked by UV light for 0s, 60s, 120s, 240s, and 480s, respectively.

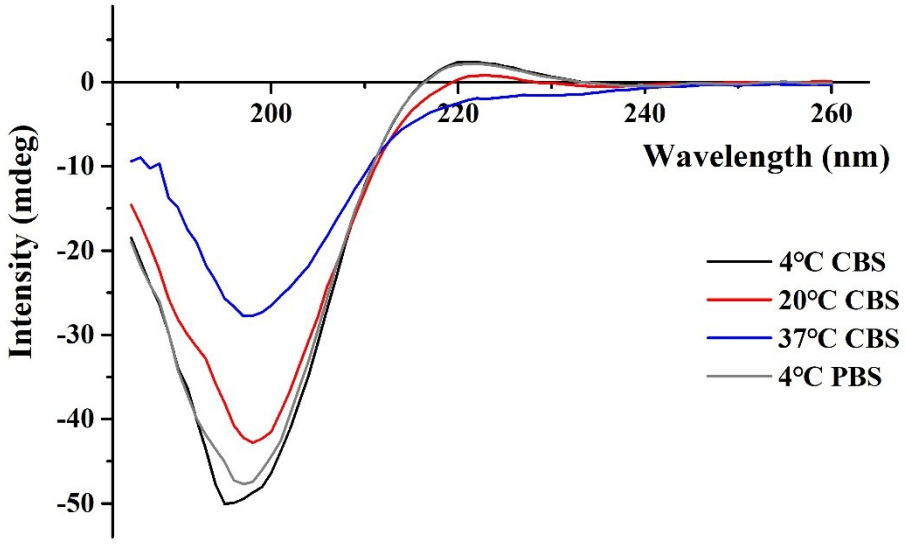

Fig.S3 CD spectra of Gel under the CBS and PBS reaction systems without the addition MA.

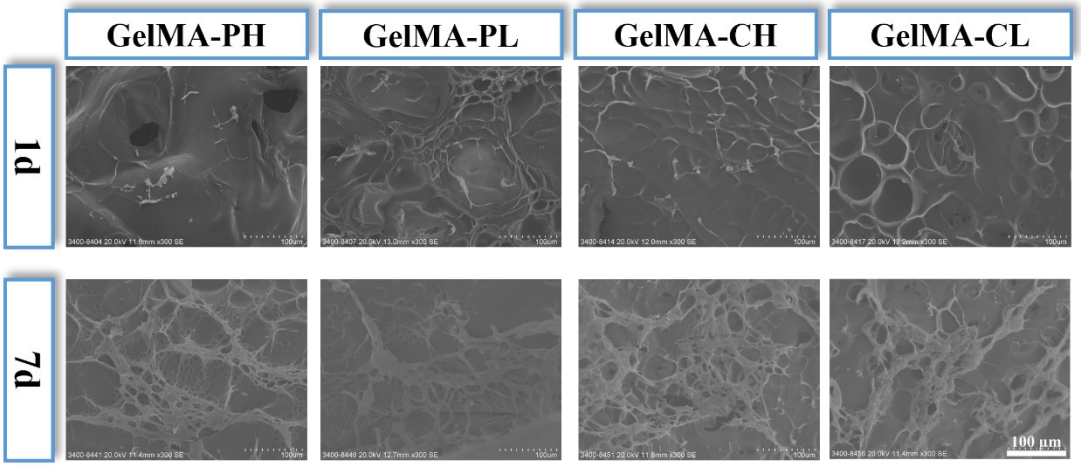

Fig.S4 SEM images showing BMSC morphology on GelMA-PH, GelMA-PL, GelMA-CH, and GelMA-CL hydrogels after cell culture for 1 and 7 days, respectively.

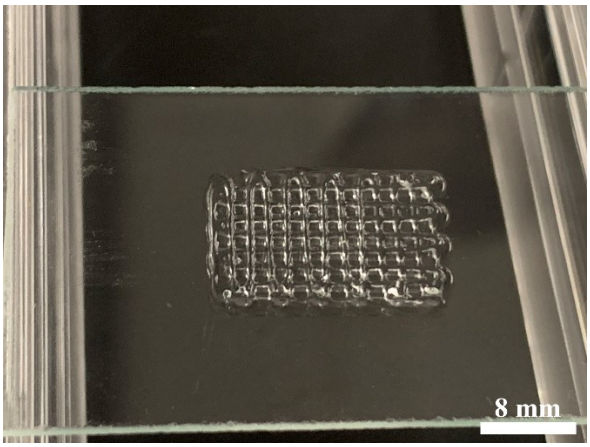

Fig.S5 A macroscopic view (a photo) of a 3D bioprinted GelMA-PH structure (4 layers) was captured using a digital camera (Nikon). 5.0 wt.% GelMA-PH bioinks were 3D printed at 20℃ to prepare BMSCs-laden hydrogel.

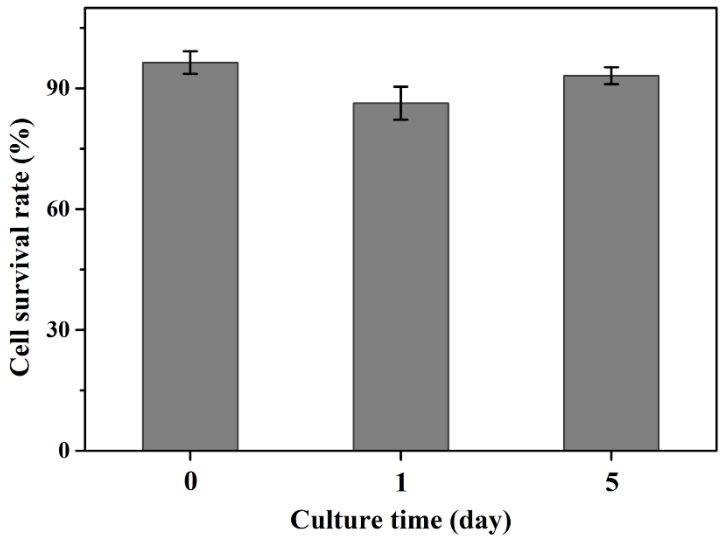

Fig.S6 Survival rate of BMSCs in 3D bioprinted GelMA-PH hydrogel after cell culture for 1 and 5 days, respectively.

Table.S1 Peak intensity at 198nm and 222nm in CD spectra of Gel, GelMA-PH, GelMA-PL, GelMA-CH, and GelMA-CL at 4℃, 20℃, and 37℃, respectively.

Material	Intensity					
	4℃		20℃		37℃	
	198nm	222nm	198nm	222nm	198nm	222nm
Gel	-51.92	2.79	-44.84	0.75	-30.18	-1.07
GelMA-PH	-41.75	1.97	-33.85	0.28	-24.80	-0.85
GelMA-PL	-45.14	2.24	-37.33	0.64	-25.80	-0.47
GelMA-CH	-34.59	-0.14	-33.19	-1.73	-25.89	-1.31
GelMA-CL	-38.07	1.45	-31.82	-0.69	-27.17	-0.52